

1 Measurement report: Brown carbon aerosol in rural Germany: 2 sources, chemistry, and diurnal variations

3 *Feng Jiang^{1,2,a*}, Harald Saathoff^{1*}, Uzoamaka Ezenobi¹, Junwei Song¹, Hengheng Zhang¹, Linyu*
4 *Gao¹, and Thomas Leisner^{1,3}*

5 ¹Institute of Meteorology and Climate Research, Karlsruhe Institute of Technology, 76344 Eggenstein–Leopoldshafen,
6 Germany

7 ²Institute of Applied Geosciences, Working Group for Environmental Mineralogy and Environmental System
8 Analysis, Karlsruhe Institute of Technology, 76131 Karlsruhe, Germany

9 ³Institute of Environmental Physics, Heidelberg University, 69120 Heidelberg, Germany

10 ^anow at: Paul H. O’Neill School of Public & Environmental Affairs, Indiana University, Bloomington, Indiana 47405,
11 United States

12 *Correspondence to:* Feng Jiang (feng.jiang@kit.edu) and Harald Saathoff (harald.saathoff@kit.edu)

13
14 **Abstract.** Brown carbon aerosol (BrC) is one major contributor to atmospheric air pollution in Europe, especially in
15 winter. Therefore, we studied the chemical composition, diurnal variation, and sources of BrC from 17th February to
16 16th March 2021 at a rural location in southwest Germany. In total, 178 potential BrC molecules (including 7 nitro
17 aromatic compounds, NACs) were identified in the particle phase comprising on average $83 \pm 44 \text{ ng m}^{-3}$, and 31
18 potential BrC (including 4 NACs) molecules were identified in the gas phase contributing on average $8.5 \pm 6.7 \text{ ng m}^{-3}$
19 during the whole campaign. The average light absorption of seven NACs in the particle phase was $0.2 \pm 0.2 \text{ Mm}^{-1}$,
20 contributing to $2.2 \pm 2.1\%$ of total BrC absorption at 370 nm. In addition, diurnal variations show that gas phase BrC
21 was higher at daytime and lower at night. It was mainly controlled by secondary formation (e.g., photooxidation) and
22 particle-to-gas partitioning. Correspondingly, the particle phase BrC was lower at daytime and higher at nighttime.
23 Secondary formation dominates the particle-phase BrC with $61 \pm 21\%$, while $39 \pm 21\%$ originated from biomass
24 burning. Furthermore, the particle-phase BrC showed decreasing light absorption due to photochemical aging. This
25 study extends the current understanding of real-time behaviors of brown carbon aerosol in the gas and particle phase
26 at a location characteristic for the central Europe.

27 **1. Introduction**

28 The Brown Carbon (BrC) aerosol has significant impact on air quality and climate, since it absorbs the solar radiation
29 in the near-ultraviolet and visible region (Laskin et al., 2015; Moise et al., 2015). Global simulation showed that the
30 mean radiative forcing of BrC aerosol was -0.43 W m^{-2} and 0.05 W m^{-2} at the surface and at the top of the atmosphere,
31 accounting for 15% of total radiative forcing by the absorbing aerosol (Park et al., 2010). In addition, global
32 measurements of BrC found that the average direct radiative effect of BrC absorption accounted between 7% to 48%
33 at the top of the atmosphere (Zeng et al., 2020).

34 Some typical molecules of BrC have been identified, such as nitro-aromatic compounds (NACs), imidazoles, and
35 polycyclic aromatic hydrocarbons (PAH), etc., (Jiang et al., 2022; Wu et al., 2018; Huang et al., 2018; Liu et al., 2023).

36 In western Europe, the concentration levels of NACs range between $1\text{--}20 \text{ ng m}^{-3}$, accounting for 0.3%–4% of total
37 absorption of BrC at UV wavelengths (Jiang et al., 2022; Mohr et al., 2013; Teich et al., 2017). In addition, imidazoles
38 were detected with concentrations ranging between $0.2\text{--}14 \text{ ng m}^{-3}$ in ambient aerosol samples from different
39 environments in Europe and China (Teich et al., 2016). Furthermore, parent-PAHs and carbonyl-OPAHs accounted
40 for on average $\sim 1.7\%$ of the overall absorption of methanol-soluble BrC in Urban Xi'an, Northwest China (Huang et
41 al., 2018). Even though many studies have investigated the chemical composition of brown carbon and calculated the
42 absorption contribution from BrC molecules, there are still many unknown brown carbon molecules to allow a
43 quantitative assessment of their sources and atmospheric impact.

44 Sources of BrC can be separated as primary emissions and secondary formation. The primary sources of BrC are
45 biomass burning and fossil fuel combustion (Andreae and Gelencser, 2006). On a global scale, a majority of BrC
46 aerosol mass is associated with biomass burning dominating BrC absorption (Zeng et al., 2020). The major secondary
47 sources of brown carbon are from oxidation of aromatic volatile organic compounds, such as toluene (Lin et al., 2015),
48 naphthalene (Siemens et al., 2022), ethylbenzene (Yang et al., 2022), and indole (Montoya-Aguilera et al., 2017; Jiang
49 et al., 2024), especially in the presence of NO_2 .

50 BrC in the atmosphere can be suspended in the gas phase or particle phase. However, only a few studies have
51 investigated the sources and chemical composition of BrC in the gas phase. For example, NACs in the gas phase were
52 highest during the daytime at a rural site in China (Salvador et al., 2021). The major sources of NACs were from
53 secondary formation on days without extensive biomass burning emissions, but mainly from primary emissions in
54 biomass burning events (Salvador et al., 2021). The source of nitrophenol, a typical BrC molecule, was mainly from
55 secondary formation outweighing losses by photolysis in polluted urban environments, Beijing (Cheng et al., 2021).

56 The major chromophores of BrC in the gas phase were rich in phenol- and protein-like substances in Xi'an, China,
57 during the summer (Chen et al., 2021). Therefore, the previous studies mainly focus on sources and chromophores of
58 BrC, especially NACs. However, the real-time diurnal variation and sources of BrC in the gas phase in the atmosphere
59 have rarely been investigated in central Europe.

60 Previous field studies have investigated the sources of BrC in the particle phase which are mainly from secondary
61 formation and primary emissions (Wang et al., 2019a; Moschos et al., 2018; Satish et al., 2017). In the central Europe,
62 the secondary biogenic organic aerosol (OA) contributes less BrC in summer. However, the primary and secondary
63 wood burning emissions dominated the BrC (Moschos et al., 2018). The primary emissions of BrC contributed more
64 to organic aerosol light absorption than those from secondary processes in the North China Plain, China (Wang et al.,
65 2019a). However, secondary sources for BrC were more important for absorption than primary ones in the Southeastern
66 Margin of Tibetan Plateau (Wang et al., 2019b). Loss pathways of BrC in the particle phase mainly comprise
67 photooxidation and photobleaching, but also dilution of BrC e.g. by rising boundary layer height influences its
68 concentration levels (Satish et al., 2017; Laskin et al., 2015; Moise et al., 2015). The absorption of BrC was high in
69 the early morning and later decreased due to the bleaching of chromophores (Wang et al., 2019a; Satish et al., 2017).
70 A diurnal cycle showed that secondary chromophores can be formed from photochemical oxidation after sunrise
71 followed by photobleaching of the chromophores under the oxidizing conditions as the day progressed (Wang et al.,
72 2019b). Lower BrC concentrations during noon were explained by the fact that planetary boundary layer heights were
73 highest during the middle of the day (Liu et al., 2023). However, also nighttime aqueous-phase chemistry can promote
74 the formation of secondary light absorbing compounds and the production of strongly absorbing particles (Wang et al.,
75 2019a). In addition, higher emissions of biomass burning BrC were observed at nighttime. Actually, the BrC in the
76 particle phase undergoes complex photochemical processing during the whole day. The time dependent sources and
77 diurnal variations of BrC in aerosol particles are still reported rarely and not well understood.

78 To better understand the chemical characterization, diurnal variation, and sources of BrC in central Europe, we
79 performed online measurements of BrC during February-March 2021 at a rural location in southwest Germany. In the
80 following, we will describe the experimental methods used in this study. Subsequently, the mass concentrations of BrC
81 in gas and particle phase will be determined. Furthermore, the contribution of BrC to light absorption in the particle
82 phase will be estimated. Then, the diurnal variations and sources of BrC in the gas and particle phase will be analyzed.
83 Finally, the atmospheric implications of our findings will be discussed.

84 **2. Experimental methods**

85 **2.1. Measurement site**

86 We performed particle and trace gas measurements from February 17th–March 16th 2021 at KIT Campus Nord, a rather
87 rural area in Germany (49°05'43.1"N 8°25'45.6"E). The sampling site is located at the building number 322 of the
88 IMK-AAF on KIT Campus Nord, as shown in Figure S1. The campus is mostly surrounded by the Hardwald forest
89 dominated by pine trees. The sampling site is also near some villages e.g. 3–4 km east of the village “Eggenstein-
90 Leopoldshafen”, 6–7 km northeast of the village “Neureut”, 3–4 km west of the village “Friedrichstal”, 4–5 km
91 northwest of the village “Stutensee”, and 5–6 km southeast of the village “Linkenheim”. Therefore, influences by
92 biomass burning emissions from wood stove combustion in these residential areas during winter time can be expected
93 (Thieringer et al., 2022). Furthermore, the city of Karlsruhe with 3000000 inhabitants is 10 km south of the
94 measurement site. The city includes industrial areas with a coal-fired power plant “Rheinhafen” and a refinery “MIRO”.
95 Therefore, the measurement site is potentially affected by different aerosol sources.

96 **2.2. Meteorological, aerosol particle, and traces gas instruments**

97 All instruments were set up in a temperature-controlled measurement building. The samples were collected above the
98 roof top about 8 m above ground level via stainless steel tubes and a PM_{2.5} and a TSP inlet as well as FEP tubes for the
99 VOC measurements. An overview of the instruments used and the parameters measured is given in Table S1 of the
100 Supplement.

101 Temperature, relative humidity (RH), pressure, wind speed, wind direction, precipitation, and global radiation were
102 measured by a meteorological sensor (WS700, Lufft GmbH; see Table S1) about 8 m above the ground level. The main
103 wind directions during the campaign were southwest, northeast, and southeast, since winds were channeled by the
104 Rhine River valley. O₃ and NO₂ were measured with standard gas monitors (Table S1). The particle number
105 concentrations (>2.5 nm) were measured by a water-based condensation particle counter (CPC3789, TSI Inc.). PM_{2.5}
106 was measured by an optical particle counter (OPC-FIDAS 200, Palas Inc.). The particle number size distributions were
107 measured by a nanoparticle sizer (NanoScan, TSI Inc.) ranging from 10-410 nm at a time resolution of 1 min. Black
108 carbon (BC) concentrations were measured with aethalometers (AE33, Aerosol Magee Scientific).

109 2.3. Online FIGAERO-CIMS measurement and identifications of potential BrC molecules

110 The individual organic compounds in both the gas and particle phase were measured with a filter inlet for gases and
111 aerosols coupled to a high-resolution time-of-flight chemical ionization mass spectrometer (FIGAERO-HR-ToF-CIMS,
112 Aerodyne Research Inc. hereafter CIMS) employing iodide (I⁻) for chemical ionization (Lopez-Hilfiker et al., 2014;
113 Jiang et al., 2022). During the gas-phase measurement, the ambient air was sampled via a fluorinated ethylene
114 propylene (FEP) tube of 4.5 m length (flow rate 8 L min⁻¹, residence time 0.9 s). At the same time, the particles were
115 collected on a Teflon (Polytetrafluoroethylene, PTFE) filter via a separate sampling port connected to a PM_{2.5} inlet
116 (total flow rate 16.7 L min⁻¹) and an 8 m long stainless-steel tube. The loading time and sampling flow of Teflon filters
117 were 30 minutes and 4 L min⁻¹, respectively. At regular intervals (46 min), the gas-phase measurement was switched
118 off and particles on the filter were desorbed by a flow of ultra-high-purity nitrogen (99.9999%) heated from room
119 temperature to 200 °C over the course of 35 min (Lopez-Hilfiker et al., 2014; Huang et al., 2019). The resulting mass
120 spectral signal evolutions as a function of desorption temperature are termed thermograms (Lopez-Hilfiker et al., 2014).
121 Integration of thermograms of individual compounds yielded their signal in counts per second, which were converted
122 to mass concentrations using an average sensitivity of 22 count s⁻¹ ppt⁻¹ (cps ppt⁻¹, ppt: parts per trillion) (Lopez-Hilfiker
123 et al., 2014). First calibrations for nitro aromatic compounds (NACs) were done directly after field campaign. However,
124 due to technical problems, the calibration of 4-nitrophenol, 4-nitrocatechol, 2-methyl-4-nitrophenol, and 4-methyl-5-
125 nitrocatechol was repeated in August 2024, as shown in the Supplement. Despite the large time between measurements
126 and second calibration, we have indications from repeated measurements of formic acid that the sensitivity of the
127 instrument didn't change substantially over this time period. Please note that this leads to an additional uncertainty of
128 about 20%. The sensitivities of our iodide CIMS for 4-nitrophenol, 4-nitrocatechol, 2-methyl-4-nitrophenol, and 4-
129 methyl-5-nitrocatechol were 18 ± 10 cps ppt⁻¹, 11 ± 7 cps ppt⁻¹, 21 ± 11 cps ppt⁻¹, and 21 ± 14 cps ppt⁻¹, respectively
130 (Figure S9). The average sensitivity of 4 NACs was 18 ± 12 cps ppt⁻¹. We used this average sensitivity to calibrate
131 other potential brown carbon molecules in this study. The sensitivity of levoglucosan was 9 ± 3 cps ppt⁻¹ in this study
132 (Figure S10). We used the sensitivity of 9 ± 3 cps ppt⁻¹ to estimate the concentrations of molecules, which are not
133 identified as potential BrC molecules.

134 During the measurements, the mass resolution of FIGAERO-CIMS was relatively stable with about 4000 m/Δ. The
135 interference from isomers with different vapor pressures or thermal fragmentation of larger oligomeric molecules can
136 lead to more complex, multimodal and broader thermograms (Lopez-Hilfiker et al., 2014). The signal integration can

137 include the different isomers or thermal fragmentation of larger oligomers. Therefore, the isomers or thermal
138 decomposition can lead to increase errors of estimating the organic mass concentrations. In this study, BrC molecules
139 were identified and partially quantified in atmospheric aerosol by FIGAERO-CIMS. Please note that the iodide CIMS
140 has sensitivities varying over several orders magnitude for different compounds e.g., of different oxidation states
141 (Lopez-Hilfiker et al., 2016). Therefore, the quantitative interpretation is limited to the small amount of compounds
142 for which we could do calibration with authentic standards. Keeping this in mind, it can still be meaning to a relative
143 comparison of the large number of high oxidized compounds assuming the same sensitivity. The raw data were
144 analysed by using the toolkit Tofware (v3.1.2, Tofwerk, Thun, Switzerland, and Aerodyne, Billerica) with the Igor Pro
145 software (v7.08, Wavemetrics, Portland, OR). Gas phase background was determined by sampling zero air (high purity
146 synthetic air). Particle phase backgrounds were assessed by putting an additional Teflon filter upstream of the particle
147 phase sampling port during the deposition (Huang et al., 2019; Lee et al., 2018).

148 We observed typically about 1500 mass peaks from particles and 120 mass peaks in gases corresponding to different
149 oxygenated organic compounds by using FIGAERO-CIMS. Individual compounds were assigned to the mass peaks
150 by fitting, $C_cH_hO_oN_n$, different numbers of atoms: c carbon, h hydrogen, o oxygen, n nitrogen (Lopez-Hilfiker et al.,
151 2014). A double bond equivalent (DBE) can be calculated as follows (Daumit et al., 2013):

$$152 \quad DBE = \frac{n-h}{2} + c + 1 \quad (1)$$

153 Lin et al., (2016, 2018) employed high-resolution mass spectrometry to analyze biomass burning organic aerosol. They
154 assigned potential brown carbon compounds according to the correlation of double bond equivalents (DBE) with the
155 number of carbon atoms per molecule (Figure S12). We used this method to assign 178 potential BrC molecules
156 (including 7 NACs) in the particle phase and 31 potential BrC molecules (including 4 NACs) in the gas phase, as
157 shown in Figure 1 in the corresponding mass spectra. The gas-to-particle phase partitioning coefficients of those semi
158 volatile potential brown carbon molecules which could be measured in both phases with sufficient sensitivity are listed
159 in table S6. A few other studies also used this method to assign more brown carbon molecules. For example, good
160 correlations ($r = 0.9$) between mass absorption efficiency at 365 nm and potential brown carbon molecules of larger
161 molecular weight were found by Tang et al. (2020). Xu et al. (2020) used this method to assign 149 nitrogen-containing
162 potential BrC chromophores at the Tibetan Plateau and we used this method to assign potential BrC molecules in
163 downtown Karlsruhe (Jiang et al., 2022). The potential BrC molecules we assigned according to this method for the
164 particle and the gas phase are listed in Tables S2 and S3.

165 2.4. Particle light absorption from aethalometer measurements

166 In the aethalometer AE33 (Magee Scientific), aerosol particles are continually sampled on a quartz filter and the optical
167 attenuation is measured with time resolutions of 1 minute at seven wavelengths (370, 470, 520, 590, 660, 880, and 950
168 nm) during this campaign. The light absorption at seven wavelengths was calculated from the measured attenuation.
169 Attenuation is measured on two spots with different sample flows and on the reference spot without sample flow. The
170 two loading spots with different flow are used to allow for loading effect corrections (Drinovec et al., 2015). Since our
171 aethalometer has been used with two loading spots, the loading effect was corrected by a Dual-spot loading
172 compensation algorithm (Drinovec et al., 2015). To further address the scattering effect (Yus-Díez et al., 2021), we
173 did comparison experiments in the Aerosol Preparation and Characterization (APC) chamber (Huang et al., 2018).
174 Black carbon was injected into the APC chamber by using the PALAS soot generator (GfG 1000, Palas) (Saathoff et
175 al., 2003). The APC chamber was connected to a photoacoustic spectrometer (PAS) operating at three wavelengths
176 (405, 520, and 658 nm) (Linke et al., 2016) and an aethalometer (AE33). As shown in Figure S11, for three wavelengths
177 (370, 520, and 660 nm), the correlation slopes were 1.88, 1.94, and 1.98, respectively. The average multiple-scattering
178 correction factor was 1.90 ± 0.06 in this study.

179 The BC mass concentration is calculated from the change in optical attenuation at 880 nm in the selected time interval
180 using the mass absorption cross section $7.77 \text{ m}^2 \text{ g}^{-1}$ (Gundel et al., 1984), since other aerosol particles (organic aerosol
181 or mineral) have less absorption at this wavelength and major absorption is contributed from BC alone. The attenuation
182 mass absorption coefficients of AE33 from 370–880 nm were 18.47, 14.54, 13.14, 11.58, 10.35, and $7.77 \text{ m}^2 \text{ g}^{-1}$,
183 respectively. The absorption measurements by an aethalometer have the filter-based lensing effect (Moschos et al.
184 2021). According to previous studies, the uncertainty from the lensing effect for BC and BrC measurement was 8%-
185 27% and 6%-20%, respectively (Moschos et al., 2021). We assumed an AAE_{BC} value of 1.0 in this study. However,
186 this assumption introduces an uncertainty in the estimations of BC and BrC light absorptions. According to previous
187 studies, the AAE_{BC} ranges between 0.8 and 1.4 (Lack and Langridge 2013). This range, although maybe not fully
188 applicable to our measurement location, potentially causes relatively large uncertainties of up to 81% (at 370 nm) in
189 splitting between BrC and BC absorption (Figure S13) (Duan et al. 2024). Despite these potentially large uncertainties
190 on absolute absorption values, we consider this method still useful. Our assumption of $\text{AAE}_{\text{BC}} = 1.0$ is reasonable for
191 our location as based on previous measurements, and it should still allow to discuss the relative evolution of BC and
192 BrC absorption.

193 We assumed that the absorption from dust and other aerosol was negligible. Hence, the absorption was only contributed
 194 from BC and BrC. Therefore, $Abs(\lambda)$ can be divided in BC and BrC absorption:

$$195 \quad Abs = Abs_{BrC}(\lambda) + Abs_{BC}(\lambda) \quad (2)$$

196 where $Abs_{BrC}(\lambda)$ is the absorption caused by BrC at the following aethalometer wavelengths, $\lambda = 370, 470, 520, 590,$
 197 or 660 nm while $Abs_{BC}(\lambda)$ is the absorption contributed by BC at the same wavelength (Wang et al., 2019a). To
 198 determine $Abs_{BC}(\lambda)$ at each wavelength, we assumed that BC was the only absorber at $\lambda = 880$ nm, and thus the $Abs_{BC}(\lambda)$
 199 ($\lambda = 370, 470, 520, 590,$ and 660) can be extrapolated from the following equation:

$$200 \quad Abs_{BC}(\lambda) = Abs_{880} \times \left(\frac{\lambda}{880}\right)^{-AAE_{BC}} \quad (3)$$

201 where AAE_{BC} represents the spectral dependence of $Abs_{BC}(\lambda)$, and a value of 1.0 was chosen for AAE_{BC} based on
 202 previous studies in Germany (Teich et al., 2017). Finally, one can obtain the $Abs_{BrC}(\lambda)$ as follows:

$$203 \quad Abs_{BrC}(\lambda) = Abs(\lambda) - Abs(880) \times \left(\frac{\lambda}{880}\right)^{-AAE_{BC}} \quad (4)$$

204 The fraction of wood burning black carbon (BC_{wb}) was calculated by using the aethalometer model (Sandradewi et
 205 al., 2008a; Sandradewi et al., 2008b):

$$207 \quad BC_{wb} = \left[\frac{b_{abs}(470nm) - b_{abs}(950nm) \times \left(\frac{470}{950}\right)^{-\alpha_{ff}}}{\left(\frac{470}{950}\right)^{-\alpha_{wb}} - \left(\frac{470}{950}\right)^{-\alpha_{ff}}} \right] / b_{abs}(950nm) * BC \quad (5)$$

208 Where two pairs of Ångström exponent values were utilized to obtain BC associated with fossil fuel (BC_{ff}) and wood
 209 burning (BC_{wb}). One of the largest sources of uncertainty in the aethalometer model is related to the section of α_{ff} and
 210 α_{wb} values (Healy et al., 2017; Zotter et al., 2017). In addition, the α_{ff} was typically in the range of ~ 0.8 – 1.2 in
 211 ambient air whereas α_{wb} can vary from 1.6 to 2.2 (Saarikoski et al., 2021). However, we used the α_{ff} and α_{wb} values
 212 as 0.95 and 1.68 to calculate the BC source (Helin et al., 2018), since our measurement site is in a rural area and nearby
 213 a suburban area.

214 **3. RESULTS AND DISCUSSION**

215 **3.1. Overview of the field observations**

216 Figures S1 and S2 give an overview of the measurement location and the meteorological parameters, traces gases,
 217 particle concentrations, and their optical properties during the campaign. The major wind directions at KIT Campus
 218 Nord, 3 km east of the village of Eggenstein-Leopoldshafen, were northeast and southwest (Figure S1) caused by
 219 channeling of the wind in the Rhine valley. The average wind speeds were 1.1 ± 0.8 (average \pm standard deviation) m

220 s⁻¹. Depending on meteorological conditions, local sources and regional transport had a major impact on air quality in
221 Leopoldshafen in summer (Shen et al., 2019). As shown in Figure S5, O₃ had diurnal variations with peaks at daytime
222 and an average of 41.3 ± 26.2 μg m⁻³ during the campaign. In contrast, the relative humidity (RH) showed diurnal
223 variations with peaks at nighttime and an average of 68 ± 16% during the campaign (Figure S5). The average
224 temperature during the winter campaign was 6.5 ± 5.6 °C and slowly increased from beginning to the end of the
225 campaign. NO₂ had high concentrations at some periods e.g., from 20th to 23rd February with 22 ± 8.6 μg m⁻³ and from
226 2nd to 4th March with 35 ± 14 μg m⁻³. The average SO₂ concentration was 0.8±1.0 μg m⁻³, significantly lower than the
227 NO₂ concentrations. During some Saharan dust events, the PM_{2.5} and PM₁₀ mass concentrations were 21 ± 6 and 45 ±
228 20 μg m⁻³, respectively, from 18th to 26th February and 19 ± 6 and 24 ± 7 μg m⁻³, respectively, from 1st to 4th March as
229 indicated by red boxes in the lowest panel of Figure S2. In addition, BC showed many spikes and a good correlation
230 (r = 0.8) with NO₂ (Figure S3). This indicates that there were many combustion events during the campaign (Figure
231 S3). The absorption Ångström exponents of particles between 370 and 520 nm (AAE₃₇₀₋₅₂₀) and AAE₆₆₀₋₉₅₀ had diurnal
232 variations with peaks at nighttime. We calculated the fraction of wood burning BC and fossil fuel BC as shown in
233 Figure S3 using the aethalometer model (Sandradewi et al., 2008a). During the winter campaign, the biomass burning
234 BC was on average 0.61 ± 0.049 μg m⁻³, mostly higher than 0.025 ± 0.027 μg m⁻³ for fossil fuel BC. The AAE₃₇₀₋₅₂₀,
235 AAE₆₆₀₋₉₅₀, biomass burning BC, and NO₂ values were enhanced from 20th to 23rd February and 2nd to 4th March. This
236 indicates that strong biomass burning (BB) events were on these days. During this winter campaign, the BrC absorption
237 accounted for ~40% of total absorption caused by BC and BrC at 370 nm. This points to the at least regional or seasonal
238 importance of BrC absorption which has an important effect on air quality and climate.

239 3.2. Mass concentrations and volatility of potential brown carbon molecules

240 Figure 2 shows an overview of levoglucosan concentrations, BC concentrations, absorption of brown carbon at 370
241 nm (b_{brC370}), AAE₃₇₀₋₅₂₀, volatility, and mass concentrations of 178 potential brown carbon molecules identified in the
242 particle phase and 31 potential brown carbon molecules in the gas phase during the whole winter campaign. We
243 identified 178 potential BrC molecules according to the method developed by Lin et al., (2018) (cf. section 2.3.). The
244 mass of these molecules shows a good correlation (r = 0.7 ± 0.1) with the absorption at 370 nm (b_{BrC370}) of BrC (sf.
245 Figure S6). This indicates that it is meaningful to extract these 178 potential BrC molecules from more than one
246 thousand and five hundred molecules detected by FIGAERO-CIMS based on the double bond equivalent/carbon
247 number ratio (DBE/C) of each molecule being higher than 0.5 and less than 0.9. The levoglucosan showed a good

248 correlation ($r = 0.7$) with BC. This is in line with the large fraction of biomass burning contributing to BC during the
249 winter campaign. Biomass burning BC accounted for $(71 \pm 40)\%$ of total BC as we discussed above. The 178 potential
250 BrC molecules detected in the particle phase correspond to an average mass concentration of $83 \pm 44 \text{ ng m}^{-3}$. In addition,
251 the nitro aromatic compounds (NACs) were also detected during the winter campaign. The mass concentrations of
252 \sum NACs in the gas phase and particle phase were $1.9 \pm 1.5 \text{ ng m}^{-3}$ and $17.5 \pm 18.4 \text{ ng m}^{-3}$, respectively (Tables S4 and
253 S5). Mohr et al. (2013) found that five BrC molecules (nitro aromatic compounds) were 20 ng m^{-3} detected by CIMS
254 during winter in Detling, United Kingdom. Jiang et al. (2022) measured an average concentration of five BrC molecules
255 (nitro aromatic compounds) of $1.6 \pm 0.9 \text{ ng m}^{-3}$ during the winter at a kerbside in downtown Karlsruhe, a city in
256 southwest Germany and close to our measurement site. Therefore, the detection of the 178 potential BrC molecules
257 allows a more complete assessment of the BrC concentrations during this winter campaign. Their concentrations were
258 significantly higher for biomass burning (BB) events e.g., $144 \pm 41 \text{ ng m}^{-3}$ at BB event 1 and $124 \pm 39 \text{ ng m}^{-3}$ at BB
259 event 2, respectively. In addition, the absorption of brown carbon at 370 nm ($b_{\text{brc}370}$) had high peaks with $\sim 100 \text{ Mm}^{-1}$
260 and the $\text{AAE}_{370-520}$ of particles increased from ~ 1.5 to ~ 2 during the BB events. The average concentration of potential
261 BrC in the gas phase was $8.5 \pm 6.7 \text{ ng m}^{-3}$ during the winter campaign. At BB events, their concentration can reach up
262 to 38 ng m^{-3} . Therefore, biomass burning had a significant impact on optical properties of aerosol and brown carbon
263 concentrations. The lowermost panel of Figure 2 shows the temporal variation of the average volatility of brown carbon
264 molecules in the gas and particle phase. The average volatility or saturation concentration ($\log_{10}C_{\text{sat}}$) of potential BrC
265 in the particle phase was $-1.1 \pm 0.5 \text{ } \mu\text{g m}^{-3}$ lower than $0.9 \pm 0.6 \text{ } \mu\text{g m}^{-3}$ of potential BrC in the gas phase during the
266 winter campaign. Organic compounds with $\log_{10}C_{\text{sat}}$ lower than $-4.5 \text{ } \mu\text{g m}^{-3}$, between -4.5 and $-0.5 \text{ } \mu\text{g m}^{-3}$, between
267 -0.5 and $2.5 \text{ } \mu\text{g m}^{-3}$, and between 2.5 and $6.5 \text{ } \mu\text{g m}^{-3}$ are termed extremely low-volatility organic compounds (ELVOCs),
268 low-volatility organic compounds (LVOCs), semi-volatile organic compounds (SVOCs), and intermediate-volatility
269 organic compounds (IVOCs), respectively (Donahue et al., 2009). Therefore, BrC in the particle phase can be classified
270 on average to the LVOCs and BrC in the gas phase to the SVOCs.

271 3.3 Absorption contribution of nitro aromatic compounds

272 Black carbon dominated light absorption of aerosol particles with a contribution of 100% at 880 nm and decreasing to
273 73% at 370 nm. With shorter wavelengths, the brown carbon absorption contribution significantly increased
274 contributing 27% of total aerosol absorption at 370 nm (Figure 3a). We calculated the average light absorption of seven
275 nitro aromatic compounds (NACs) by using the mass absorption coefficients (MAC_{365} , Xie et al., 2017), given in Table

276 S5 and the average concentrations measured. Based on this, the mean light absorption of the sum of the seven NACs
277 was calculated to be $0.2 \pm 0.2 \text{ Mm}^{-1}$. The absorption of the seven NACs contributed to $2.2 \pm 2.1\%$ of total BrC
278 absorption at 370 nm (Figure 3b). Palm et al. (2020) found that particulate nitroaromatic compounds (BrC molecules)
279 can explain $29 \pm 15\%$ of average BrC light absorption at 405 nm, despite accounting for just $4 \pm 2\%$ of average OA
280 mass in fresh wildfire plumes. Mohr et al. (2013) found that five nitroaromatic compounds (BrC molecules) are
281 potentially important contributors to absorption at 370 nm measured by an aethalometer and account for $4 \pm 2\%$ of UV
282 light absorption by brown carbon in Detling, United Kingdom during winter. Jiang et al. (2022) determined a mean
283 light absorption of five nitro aromatic compounds accounting for $0.3 \pm 0.1\%$ of methanol-soluble BrC absorption at
284 365 nm, but only accounted for $0.03 \pm 0.01\%$ of the organic aerosol mass. Therefore, NACs are typical brown carbon
285 molecules with typically lower mass contributions to total organic aerosol but relatively higher contributions to the
286 total BrC absorption.

287 **3.4 Diurnal variations and sources of potential BrC in the gas phase**

288 As shown in Figure 4a, the 31 gas-phase potential BrC (GBrC) molecules showed higher concentrations at daytime
289 (09:00-17:00) and lower concentrations between evening and early morning (18:00-08:00). Salvador et al. (2021) also
290 found that 16 gas-phase nitro-aromatic compounds (BrC molecules) measured by FIGAERO-CIMS were higher during
291 daytime and lower at nighttime during winter in rural China. As discussed above, strong biomass burning emissions
292 were mostly observed at evening and early morning hours. However, gas-phase BrC had no peaks during those time
293 periods. Therefore, the primary emission from biomass burning was not a major source for GBrC at KIT Campus Nord.
294 It seems to be mainly controlled by secondary formation (e.g., photochemical smog) or/and particle-to-gas partitioning
295 (Salvador et al., 2021).

296 To demonstrate how secondary formation and partitioning control the gas-phase BrC in rural Germany, we plotted
297 diurnal profiles of the average volatility and volatility fractions of IVOC, SVOC, and LVOC of the gas-phase BrC
298 (Figure 4b). The LVOC of BrC increased at evenings and decreased at daytime. In contrast, the IVOC of BrC increased
299 at daytime and reached $\sim 17\%$ of total $\log_{10}C^*$ (volatility) in gas-phase BrC while SVOC remained with a relative
300 constant fraction ($\sim 60\%$). Furthermore, the IVOC fraction of BrC in the particle phase was only 1.5% with a flat diurnal
301 profile (Figure S7). The O/C ratio of gas-phase BrC also increased during daytime (Figure 4d). Therefore, the higher
302 fraction of IVOC in the gas phase at daytime is most likely caused by secondary formation e.g., photochemical
303 conversion/aging because of higher oxidant levels as indicated e.g., by higher concentration of ozone at same time

304 (Figure 4c) (Saarikoski et al., 2021). Figure S8 shows that BrC in the gas phase had a moderate positive correlation (r
305 = 0.4) with temperature. This explains why the temperature shows a similar diurnal profile as the gas-phase BrC.
306 Therefore, particle-to-gas partitioning was also an important source for gas-phase BrC. However, our results are not
307 consistent with previous studies where 16 BrC molecules in gas phase were mainly from primary emission during the
308 biomass burning evenings and secondary formation during the clear days in rural China (Salvador et al., 2021). Our
309 measurement site was several km away from biomass burning sites with ~7-10 km. And the 31 potential BrC in the
310 gas phase sum up to $8.5 \pm 6.7 \text{ ng m}^{-3}$, significantly lower than 1720 ng m^{-3} of 16 BrC (Salvador et al., 2021). Cheng et
311 al. (2021) found that secondary formation was a strong source for five BrC molecules in the gas phase. Therefore, BrC
312 in the gas phase are less influenced by primary emissions from biomass burning but are mainly controlled by secondary
313 formation and partitioning in rural Germany.

314 **3.5 Diurnal variations and sources of potential BrC in the particle phase**

315 The 178 potential BrC molecules in the particle phase (PBrC) exhibited two peaks in the diurnal profile (Figure 4a)
316 averaged over the whole winter campaign. They increased from 19:00 to 01:00 with a peak at $82 \pm 35 \text{ ng m}^{-3}$ around
317 midnight. Then the PBrC slowly decreased after midnight. However, they increased again from 6:00 to 08:00 and
318 forming a second peak with $102 \pm 49 \text{ ng m}^{-3}$ in the morning. During daytime, they decreased reaching the lowest values
319 with $61 \pm 31 \text{ ng m}^{-3}$ at 14:00-15:00. During the nighttime and morning hours, the higher mass concentrations of PBrC
320 were caused by residential wood burning emissions. Consistently, higher $\text{PM}_{2.5}$ concentration levels at nighttime at a
321 rural site near Karlsruhe, Germany, could be assigned to wood burning emissions from wood stove operation during
322 winter (Thieringer et al., 2022). The low mass concentrations of PBrC at daytime could be explained by photobleaching
323 and evaporation of BrC, and/or dilution by the increasing planetary boundary layer heights (Satish et al., 2017). Satish
324 et al. (2017) found that BrC over the Indo-Gangetic Plain had two peaks of BrC at evening and morning hours, and
325 lowest values during daytime.

326 To determine the sources of brown carbon, we used the edge approach (Day et al., 2015). It allows to estimate the
327 contribution of primary biomass burning (BB) to the measured BrC concentrations using levoglucosan as a primary
328 source tracer. This approach is analogous to the widely used elemental carbon (EC) tracer approach, in which EC is
329 used to distinguish the primary organic carbon (POC) and secondary organic carbon (SOC) in total organic carbon
330 (OC) measurements (Day et al., 2015; Cabada et al., 2004). Levoglucosan (lev) and potential BrC were measured
331 online by the same instruments and under the same conditions. As discussed above, we observed a good correlation (r

332 = 0.8) between levoglucosan and BC during the winter campaign. Therefore, levoglucosan is a suitable tracer for
 333 primary BB. Please note that we did not calibrate the sensitivities of levoglucosan detected by FIGAERO-CIMS.
 334 Therefore, it could cause some uncertainties to estimate brown carbon from biomass burning and secondary formation.
 335 Figure 5a shows that the blue points can be used as edge points to determine the ratio of BrC/levoglucosan at the
 336 primary emissions from biomass burning. The relative contributions of primary emissions (BB) and secondary (sec)
 337 formation for total BrC molecules were estimated using the following expression:

$$338 \quad BrC_{BB} = \left(\frac{[BrC]}{[lev]_{BB}} \right) * [lev.]$$

$$339 \quad [BrC_{sec}] = [BrC_{Tot}] - [BrC_{BB}]$$

340 Where $([BrC]/[lev])_{BB}$ is the ratio of the concentration of the BrC to that of levoglucosan in the primary emissions from
 341 biomass burning and this value is 1.1 ± 0.1 (Figure 5a), BrC_{BB} and BrC_{sec} are the fractions of BrC generated through
 342 biomass burning and secondary production, respectively. BrC_{Tot} and $lev.$ are the measured concentrations of BrC and
 343 levoglucosan during the winter campaign. Using this approach, we calculated the diurnal profiles of BrC from primary
 344 emissions (BrC_{BB}) and secondary formation (BrC_{sec}) shown in Figure 5b. The uncertainty of the splitting between BrC
 345 from biomass burning and of secondary origin is mainly based on the levoglucosan concentration for which we have
 346 included the calibration. Based on this we estimated the uncertainty of the BrC source splitting to $\pm 35\%$. The mass
 347 fraction of BrC_{sec} increased at daytime and decreased at evening. This indicates that the secondary formation for BrC
 348 in the particle phase was enhanced during daytime, facilitated by the higher levels of oxidants e.g., O_3 (Figure 4c). The
 349 mass fraction of BrC_{BB} had two peaks at early morning and in the evening hours, respectively. This may be caused by
 350 residential wood burning emissions. BrC_{BB} accounts for $39 \pm 21\%$ of the total BrC as averaged for the whole
 351 measurement period. During biomass burning events, the BrC_{BB} is a major mass fraction for total BrC that accounts
 352 for $61 \pm 13\%$ during BB-event1 and $65 \pm 12\%$ during BB-event-2, respectively. Therefore, the primary emissions of
 353 BrC have a significant impact on BrC, especially, at biomass burning events. However, on average over the whole
 354 campaign, BrC_{sec} dominates the mass fraction of BrC with $61 \pm 21\%$. Therefore, the secondary formation can be
 355 considered as an important source for BrC in rural Germany. Consistently, secondary formation from biomass burning
 356 emission is important for the brown carbon absorption in the Switzerland, the central Europe. (Moschos et al., 2018).
 357 Secondary sources for BrC were more important for absorption than primary ones in the Southeastern Margin of the
 358 Tibetan Plateau (Wang et al., 2019b).

359 To further investigate the oxidation of BrC in the particle phase we plotted, the diurnal profiles of O/C ratios of BrC
360 during the whole campaign was measured, as shown in Figure 6. The O/C ratio of the potential BrC molecules increased
361 during daytime and decreased at nighttime. This is an indication for an impact of photo-oxidation on BrC either during
362 formation or aging leading to an increase of its O/C ratio. Consequently, the O/C ratio of the potential BrC molecules
363 shows a positive correlation ($r = 0.8$) with ozone, another product of photo chemistry. In contrast, the light absorption
364 of BrC at 370 nm ($b_{\text{brc}370}$) and the double bond equivalent (DBE) decreased at daytime and increased at nighttime.
365 During daytime, the absorption of brown carbon at 370 nm decreased due to lower DBE and higher O/C values of
366 brown carbon caused by photooxidation. This is in accordance with previous studies where atmospheric photooxidation
367 diminishes light absorption of primary brown carbon aerosol from biomass burning (Sumlin et al., 2017). Oxidative
368 whitening can reduce light absorption of brown carbon during the day (Hems et al., 2021).

369 **Conclusions**

370 The chemical composition, diurnal variation, and sources of brown carbon aerosol were investigated during February-
371 March 2021 in a rural area, at KIT Campus Nord, a location characteristic for central Europe. The 178 potential brown
372 carbon molecules (including 7 nitro aromatic compounds, NACs) identified in the particle phase contributed on average
373 $83 \pm 44 \text{ ng m}^{-3}$ and 31 potential brown carbon molecules (including 4 NACs) identified in the gas phase contributed
374 on average $8.5 \pm 6.7 \text{ ng m}^{-3}$ during the whole campaign. During dedicated biomass burning events, potential BrC
375 concentrations in the particle phase were significantly higher with up to $\sim 254 \text{ ng m}^{-3}$. The average light absorption of
376 seven NACs in the particle phase was $0.2 \pm 0.2 \text{ Mm}^{-1}$, contributing to $2.2 \pm 2.1\%$ of total BrC absorption at 370 nm.
377 This shows that NACs are important molecules for brown carbon. This indicates the great importance of identifying
378 these molecules, the strong absorbers, to predict aerosol absorption.

379 Diurnal variations show that the particle-phase potential BrC had two peaks at early morning and evening hours,
380 respectively. These were mainly caused by residential wood burning emissions. In contrast, the gas-phase potential
381 BrC showed higher concentrations at daytime and lower concentrations at nighttime. The gas-phase BrC molecules
382 were mainly controlled by secondary formation (e.g., by photochemical processes) and particle-to-gas partitioning.
383 The two main sources contributed to particle-phase BrC were primary emission from biomass burning and secondary
384 formation. Secondary formation, e.g. by photooxidation, is an important source of particle-phase BrC corresponding
385 to increasing O/C ratios of BrC during daytime and a positive correlation ($r = 0.8$) with ozone concentrations. In

386 addition, the DBE of the particle phase decreased during daytime. This indicates that the absorption of brown carbon
387 at 370 nm decreased due to lower DBE and a higher O/C ratio due to the photooxidation of brown carbon. Compared
388 with previous measurements in central Europe (Lukács et al., 2007; Zhang et al., 2020), our study found that secondary
389 formation, e.g., photochemical processes, was an important source for BrC in gas and particle phases. To improve air
390 quality in winter, we need to reduce biomass burning emissions (e.g., regulate wood stoves) but also reduce the
391 precursors to form secondary aerosol. Overall, this study provides good insight into the light absorption, sources, and
392 diurnal variation from real-time observations of brown carbon molecules in central Europe by using mass spectrometry
393 and an aethalometer.

394 *Data availability*

395 The data related to this article are accessible at KIT open data (<https://doi.org/10.35097/d0prpzqxqkq2t09y>, Jiang et
396 al., 2024).

397 **Competing interests**

398 At least one of the (co-)authors is a member of the editorial board of Atmospheric Chemistry and Physics.

399 **Author contributions**

400 FJ and HS designed the measurement campaign. FJ, LG, JS, and HS performed the experimental work. FJ did
401 FIGAERO-CIMS and AE33 data analysis. HS and HZ processed the trace gas and meteorological data, respectively.
402 UE did CIMS sensitivity calibrations. TL gave general comments for this paper. FJ wrote the paper with contributions
403 from all co-authors.

404 **ACKNOWLEDGMENTS**

405 The authors gratefully thank the staff of IMK-AAF for providing substantial technical support during the field
406 campaigns under COVID conditions. Furthermore, Feng Jiang and Junwei Song are thankful for the support from the
407 China Scholarship Council (CSC).

408

409 REFERENCES

- 410 Andreae, M. O., and Gelencser, A.: Black carbon or brown carbon? The nature of light-absorbing carbonaceous
411 aerosols, *Atmos. Chem. Phys.*, 6, 3131-3148, <https://doi.org/10.5194/acp-6-3131-2006>, 2006.
- 412 Cabada, J. C., Pandis, S. N., Subramanian, R., Robinson, A. L., Polidori, A., and Turpin, B.: Estimating the secondary
413 organic aerosol contribution to PM_{2.5} using the EC tracer method, *Aerosol Sci. Technol.*, 38, 140-155,
414 <https://doi.org/10.1080/02786820390229084>, 2004.
- 415 Chen, Q. C., Chen, Q., Hua, X. Y., Guan, D. J., and Chang, T.: Gas-phase brown carbon: Absorbance and chromophore
416 types, *Atmos. Environ.*, 264, 118646, <https://doi.org/10.1016/j.atmosenv.2021>, 2021.
- 417 Cheng, X., Chen, Q., Li, Y., Huang, G., Liu, Y., Lu, S., Zheng, Y., Qiu, W., Lu, K., Qiu, X., Bianchi, F., Yan, C.,
418 Yuan, B., Shao, M., Wang, Z., Canagaratna, M. R., Zhu, T., Wu, Y., and Zeng, L.: Secondary Production of Gaseous
419 Nitrated Phenols in Polluted Urban Environments, *Environ. Sci. Technol.*, 55, 4410-4419,
420 <https://doi.org/10.1021/acs.est.0c07988>, 2021.
- 421 Daumit, K. E., Kessler, S. H., and Kroll, J. H.: Average chemical properties and potential formation pathways of highly
422 oxidized organic aerosol, *Farad. Disc.*, 165, 181-202, <https://doi.org/10.1039/c3fd00045a>, 2013.
- 423 Day, M. C., Zhang, M. H., and Pandis, S. N.: Evaluation of the ability of the EC tracer method to estimate secondary
424 organic carbon, *Atmos. Environ.*, 112, 317-325, <https://doi.org/10.1016/j.atmosenv.2015.04.044>, 2015.
- 425 Donahue, N. M., Robinson, A. L., and Pandis, S. N.: Atmospheric organic particulate matter: From smoke to secondary
426 organic aerosol, *Atmos. Environ.*, 43, 94-106, <https://doi.org/10.1016/j.atmosenv.2008.09.055>, 2009.
- 427 Drinovec, L., Mocnik, G., Zotter, P., Prevot, A. S. H., Ruckstuhl, C., Coz, E., Rupakheti, M., Sciare, J., Muller, T.,
428 Wiedensohler, A., and Hansen, A. D. A.: The "dual-spot" Aethalometer: an improved measurement of aerosol black
429 carbon with real-time loading compensation, *Atmos. Meas. Tech.*, 8, 1965-1979, [https://doi.org/10.5194/amt-8-1965-](https://doi.org/10.5194/amt-8-1965-2015)
430 2015, 2015.
- 431 Jing, D., Huang, R., Lin, C., Shen, J., Yang, L., Yuan, W., Wang, Y., Liu, Y., and Xu W.: Aromatic Nitration Enhances
432 Absorption of Biomass Burning Brown Carbon in an Oxidizing Urban Environment, *Environ. Sci. Technol.*, 58, 17344-
433 54, <https://doi.org/10.1021/acs.est.4c05558>, 2024.
- 434 Gundel, L. A., Dod, R. L., Rosen, H., and Novakov, T.: The relationship between optical attenuation and black carbon
435 concentration for ambient and source particles, *Sci. Total Environ.*, 36, 197-202, [https://doi.org/10.1016/0048-](https://doi.org/10.1016/0048-9697(84)90266-3)
436 9697(84)90266-3, 1984.
- 437 Healy, R. M., U. Sofowote, Y. Su, J. Deboz, M. Noble, C. H. Jeong, J. M. Wang, N. Hilker, G. J. Evans, G. Doerksen,
438 K. Jones, and A. Munoz.: Ambient measurements and source apportionment of fossil fuel and biomass burning black
439 carbon in Ontario, *Atmos. Environ.*, 161, 34-47, <https://doi.org/10.1016/j.atmosenv.2017.04.034>, 2017.

440 Helin, A., Niemi, J. V., Virkkula, A., Pirjola, L., Teinilä, K., Backman, J., Aurela, M., Saarikoski, S., Rönkkö, T.,
441 Asmi, E., and Timonen, H.: Characteristics and source apportionment of black carbon in the Helsinki metropolitan
442 area, Finland, *Atmos. Environ.*, 190, 87-98, <https://doi.org/10.1016/j.atmosenv.2018.07.022>, 2018.

443 Hems, R. F., Schnitzler, E. G., Liu-Kang, C., Cappa, C. D., and Abbatt, J. P. D.: Aging of Atmospheric Brown Carbon
444 Aerosol, *ACS Earth Space Chem.*, 5, 722-748, <https://doi.org/10.1021/acsearthspacechem.0c00346>, 2021.

445 Huang, R.-J., Yang, L., Cao, J., Chen, Y., Chen, Q., Li, Y., Duan, J., Zhu, C., Dai, W., Wang, K., Lin, C., Ni, H.,
446 Corbin, J. C., Wu, Y., Zhang, R., Tie, X., Hoffmann, T., O'Dowd, C., and Dusek, U.: Brown Carbon Aerosol in Urban
447 Xi'an, Northwest China: The Composition and Light Absorption Properties, *Environ. Sci. Technol.*, 52, 6825-6833,
448 <https://doi.org/10.1021/acs.est.8b02386>, 2018.

449 Huang, W., Saathoff, H., Pajunaja, A., Shen, X., Naumann, K.H., Wagner, R., Virtanen, A., Leisner, T., and Mohr, C.:
450 alpha-Pinene secondary organic aerosol at low temperature: chemical composition and implications for particle
451 viscosity, *Atmos. Chem. Phys.*, 18, 2883-98, <https://doi.org/10.5194/acp-18-2883-2018>, 2018.

452 Huang, W., Saathoff, H., Shen, X., Ramisetty, R., Leisner, T., and Mohr, C.: Chemical Characterization of Highly
453 Functionalized Organonitrates Contributing to Night-Time Organic Aerosol Mass Loadings and Particle Growth,
454 *Environ. Sci. Technol.*, 53, 1165-1174, <https://doi.org/10.1021/acs.est.8b05826>, 2019.

455 Jiang, F., Song, J. W., Bauer, J., Gao, L. Y., Vallon, M., Gebhardt, R., Leisner, T., Norra, S., and Saathoff, H.:
456 Chromophores and chemical composition of brown carbon characterized at an urban kerbside by excitation-emission
457 spectroscopy and mass spectrometry, *Atmos. Chem. Phys.*, 22, 14971-14986, [https://doi.org/10.5194/acp-22-14971-](https://doi.org/10.5194/acp-22-14971-2022)
458 [2022](https://doi.org/10.5194/acp-22-14971-2022), 2022.

459 Jiang, F., Siemens, K., Linke, C., Li, Y., Gong, Y., Leisner, T., Laskin, A., and Saathoff, H.: Molecular analysis of
460 secondary organic aerosol and brown carbon from the oxidation of indole, *Atmos. Chem. Phys.*, 24(4), 2639-2649.
461 <https://doi.org/10.5194/acp-24-2639-2024>, 2024.

462 Jiang, F., Saathoff, H., Ezenobi, U., Song, J., Zhang, H., Gao, L., and Leisner, T.: Dataset for the publication: Brown
463 carbon aerosol in rural Germany: sources, chemistry, and diurnal variations, Karlsruhe Institute of Technology [data
464 set], <https://doi.org/10.35097/d0prpzxkxqkq2t09y>, 2024.

465 Lack, D. A., and Langridge, J. M.: On the attribution of black and brown carbon light absorption using the Ångström
466 exponent, *Atmos. Chem. Phys.*, 13, 10535-43, <https://doi.org/10.5194/acp-13-10535-2013>, 2013.

467 Laskin, A., Laskin, J., and Nizkorodov, S. A.: Chemistry of Atmospheric Brown Carbon, *Chem. Rev.*, 115, 4335-4382,
468 <https://doi.org/10.1021/cr5006167>, 2015.

469 Lee, B., Lopez-Hilfiker, F. D., D'Ambro, E. L., Zhou, P. T., Boy, M., Petaja, T., Hao, L. Q., Virtanen, A., and Thornton,
470 J. A.: Semi-volatile and highly oxygenated gaseous and particulate organic compounds observed above a boreal forest
471 canopy, *Atmos. Chem. Phys.*, 11547-11562, <https://doi.org/10.5194/acp-18-11547-2018>, 2018.

472 Lin, P., Liu, J., Shilling, J. E., Kathmann, S. M., Laskin, J., and Laskin, A.: Molecular characterization of brown carbon
473 (BrC) chromophores in secondary organic aerosol generated from photo-oxidation of toluene, *Phys. Chem. Chem.*
474 *Phys.*, 17, 23312-23325, <https://doi.org/10.1039/c5cp02563j>, 2015.

475 Lin, P., Aiona, P. K., Li, Y., Shiraiwa, M., Laskin, J., Nizkorodov, S. A., and Laskin, A.: Molecular Characterization
476 of Brown Carbon in Biomass Burning Aerosol Particles, *Environ. Sci. Technol.*, 50, 11815-24,
477 <https://doi.org/10.1021/acs.est.6b03024>, 2016.

478 Lin, P., Fleming, L. T., Nizkorodov, S. A., Laskin, J., and Laskin, A.: Comprehensive Molecular Characterization of
479 Atmospheric Brown Carbon by High Resolution Mass Spectrometry with Electrospray and Atmospheric Pressure
480 Photoionization, *Anal. Chem.*, 90, 12493-502, <https://doi.org/10.1021/acs.analchem.8b02177>, 2018.

481 Linke, C., Ibrahim, I., Schleicher, N., Hitzenberger, R., Andreae, M. O., Leisner, T., and Schnaiter, M.: A novel single-
482 cavity three-wavelength photoacoustic spectrometer for atmospheric aerosol research, *Atmos. Meas. Tech.*, 9, 5331-
483 46, <https://doi.org/10.5194/amt-9-5331-2016>, 2016.

484 Liu, X., Wang, H., Wang, F., Lv, S., Wu, C., Zhao, Y., Zhang, S., Liu, S., Xu, X., Lei, Y., and Wang, G.: Secondary
485 Formation of Atmospheric Brown Carbon in China Haze: Implication for an Enhancing Role of Ammonia, *Environ.*
486 *Sci. Technol.*, 57, 11163-11172, <https://doi.org/10.1021/acs.est.3c03948>, 2023.

487 Lukács, H., Gelencsér, A., Hammer, S., Puxbaum, H., Pio, C., Legrand, M., Kasper-Giebl, A., Handler, M., Limbeck,
488 A., Simpson, D., and Preunkert, S.: Seasonal trends and possible sources of brown carbon based on 2-year aerosol
489 measurements at six sites in Europe, *J. Geophys. Res.*, 112, <https://doi.org/10.1029/2006JD008151>, 2007.

490 Lopez-Hilfiker, F. D., Mohr, C., Ehn, M., Rubach, F., Kleist, E., Wildt, J., Mentel, T. F., Lutz, A., Hallquist, M.,
491 Worsnop, D., and Thornton, J. A.: A novel method for online analysis of gas and particle composition: description and
492 evaluation of a Filter Inlet for Gases and AEROSols (FIGAERO), *Atmos. Meas. Tech.*, 7, 983-1001,
493 <https://doi.org/10.5194/amt-7-983-2014>, 2014.

494 Lopez-Hilfiker, F. D., Iyer, S., Mohr, C., Lee, B. H., D'Ambro, E. L., Kurten, T., and Thornton, J. A.: Constraining the
495 sensitivity of iodide adduct chemical ionization mass spectrometry to multifunctional organic molecules using the
496 collision limit and thermodynamic stability of iodide ion adducts, *Atmos. Meas. Tech.*, 9, 1505-12,
497 <https://doi.org/10.5194/amt-9-1505-2016>, 2016.

498 Mohr, C., Lopez-Hilfiker, F. D., Zotter, P., Prevot, A. S. H., Xu, L., Ng, N. L., Herndon, S. C., Williams, L. R., Franklin,
499 J. P., Zahniser, M. S., Worsnop, D. R., Knighton, W. B., Aiken, A. C., Gorkowski, K. J., Dubey, M. K., Allan, J. D.,
500 and Thornton, J. A.: Contribution of Nitrated Phenols to Wood Burning Brown Carbon Light Absorption in Detling,
501 United Kingdom during Winter Time, *Environ. Sci. Technol.*, 47, 6316-6324, <https://doi.org/10.1021/es400683v>, 2013.

502 Moise, T., Flores, J. M., and Rudich, Y.: Optical Properties of Secondary Organic Aerosols and Their Changes by
503 Chemical Processes, *Chem. Rev.*, 115, 4400-4439, <https://doi.org/10.1021/cr5005259>, 2015.

504 Montoya-Aguilera, J., Horne, J. R., Hinks, M. L., Fleming, L. T., Perraud, V., Lin, P., Laskin, A., Laskin, J., Dabdub,
505 D., and Nizkorodov, S. A.: Secondary organic aerosol from atmospheric photooxidation of indole, *Atmos. Chem. Phys.*,
506 17, 11605-11621, <https://doi.org/10.5194/acp-17-11605-2017>, 2017.

507 Moschos, V., Kumar, N. K., Daellenbach, K. R., Baltensperger, U., Prevot, A. S. H., and El Haddad, I.: Source
508 Apportionment of Brown Carbon Absorption by Coupling Ultraviolet-Visible Spectroscopy with Aerosol Mass
509 Spectrometry, *Environ. Sci. Tech. Let.*, 5, 302-308, <https://doi.org/10.1021/acs.estlett.8b00118>, 2018.

510 Moschos, V., Gysel-Beer, M., Modini, R. L., Corbin, J. C., Massabo, D., Costa, C., Danelli, S. G., Vlachou, A.,
511 Daellenbach, K. R., Szidat, S., Prati, P., Prevot, A. S. H., Baltensperger, U., and El Haddad, I.: Source-specific light
512 absorption by carbonaceous components in the complex aerosol matrix from yearly filter-based measurements, *Atmos.*
513 *Chem. Phys.*, 21, 12809-12833, <https://doi.org/10.5194/acp-21-12809-2021>, 2021.

514 Palm, B. B., Peng, Q. Y., Fredrickson, C. D., Lee, B., Garofalo, L. A., Pothier, M. A., Kreidenweis, S. M., Farmer, D.
515 K., Pokhrel, R. P., Shen, Y. J., Murphy, S. M., Permar, W., Hu, L., Campos, T. L., Hall, S. R., Ullmann, K., Zhang,
516 X., Flocke, F., Fischer, E. V., and Thornton, J. A.: Quantification of organic aerosol and brown carbon evolution in
517 fresh wildfire plumes, *P. Natl. Acad. Sci. USA.*, 117, 29469-29477, <https://doi.org/10.1073/pnas.2012218117>, 2020.

518 Park, R. J., Kim, M. J., Jeong, J. I., Youn, D., and Kim, S.: A contribution of brown carbon aerosol to the aerosol light
519 absorption and its radiative forcing in East Asia, *Atmos. Environ.*, 44, 1414-1421,
520 <https://doi.org/10.1016/j.atmosenv.2010.01.042>, 2010.

521 Saarikoski, S., Niemi, J. V., Aurela, M., Pirjola, L., Kousa, A., Ronkko, T., and Timonen, H.: Sources of black carbon
522 at residential and traffic environments obtained by two source apportionment methods, *Atmos. Chem. Phys.*, 21,
523 14851-14869, <https://doi.org/10.5194/acp-21-14851-2021>, 2021.

524 Saathoff, H., Naumann, K. H., Schnaiter, M., Schöck, W., Möhler, O., Schurath, U., Weingartner, E., Gysel, M., and
525 Baltensperger, U.: Coating of soot and (NH₄)₂SO₄ particles by ozonolysis products of α -pinene, *J. Aerosol Sci.*, 34,
526 1297-321, [https://doi.org/10.1016/S0021-8502\(03\)00364-1](https://doi.org/10.1016/S0021-8502(03)00364-1), 2003.

527 Salvador, C. M. G., Tang, R. Z., Priestley, M., Li, L. J., Tsiligiannis, E., Le Breton, M., Zhu, W. F., Zeng, L. M., Wang,
528 H., Yu, Y., Hu, M., Guo, S., and Hallquist, M.: Ambient nitro-aromatic compounds - biomass burning versus secondary
529 formation in rural China, *Atmos. Chem. Phys.*, 21, 1389-1406, <https://doi.org/10.5194/acp-21-1389-2021>, 2021.

530 Sandradewi, J., Prevot, A. S. H., Szidat, S., Perron, N., Alfarra, M. R., Lanz, V. A., Weingartner, E., and Baltensperger,
531 U.: Using aerosol light absorption measurements for the quantitative determination of wood burning and traffic
532 emission contributions to particulate matter, *Environ. Sci. Technol.*, 42, 3316-3323,
533 <https://doi.org/10.1021/es702253m>, 2008a.

534 Sandradewi, J., Prevot, A. S. H., Weingartner, E., Schmidhauser, R., Gysel, M., and Baltensperger, U.: A study of
535 wood burning and traffic aerosols in an Alpine valley using a multi-wavelength Aethalometer, *Atmos. Environ.*, 42,
536 101-112, <https://doi.org/10.1016/j.atmosenv.2007.09.034>, 2008b.

537 Satish, R., Shamjad, P., Thamban, N., Tripathi, S., and Rastogi, N.: Temporal Characteristics of Brown Carbon over
538 the Central Indo-Gangetic Plain, *Environ. Sci. Technol.*, 51, 6765-6772, <https://doi.org/10.1021/acs.est.7b00734>, 2017.

539 Shen, X. L., Vogel, H., Vogel, B., Huang, W., Mohr, C., Ramisetty, R., Leisner, T., Prévôt, A. S. H., and Saathoff, H.:
540 Composition and origin of PM_{2.5} aerosol particles in the upper Rhine valley in summer. *Atmos. Chem. Phys.*, 19,
541 13189-13208. <https://doi.org/10.5194/acp-19-13189-2019>, 2019.

542 Siemens, K., Morales, A., He, Q., Li, C., Hettiyadura, A. P. S., Rudich, Y., and Laskin, A.: Molecular Analysis of
543 Secondary Brown Carbon Produced from the Photooxidation of Naphthalene, *Environ. Sci. Technol.*, 56, 3340-3353,
544 <https://doi.org/10.1021/acs.est.1c03135>, 2022.

545 Sumlin, B. J., Pandey, A., Walker, M. J., Pattison, R. S., Williams, B. J., and Chakrabarty, R. K.: Atmospheric
546 Photooxidation Diminishes Light Absorption by Primary Brown Carbon Aerosol from Biomass Burning, *Environ. Sci.*
547 *Technol. Lett.*, 4, 540-545, <https://doi.org/10.1021/acs.estlett.7b00393>, 2017.

548 Tang, J., Li, J., Su, T., Han, Y., Mo, Y. Z., Jiang, H. X., Cui, M., Jiang, B., Chen, Y. J., Tang, J. H., Song, J. Z., Peng,
549 P. A., and Zhang, G.: Molecular compositions and optical properties of dissolved brown carbon in biomass burning,
550 coal combustion, and vehicle emission aerosols illuminated by excitation-emission matrix spectroscopy and Fourier
551 transform ion cyclotron resonance mass spectrometry analysis, *Atmos. Chem. Phys.*, 20, 2513–2532,
552 <https://doi.org/10.5194/acp-20-2513-2020>, 2020.

553 Teich, M., van Pinxteren, D., Kecorius, S., Wang, Z. B., and Herrmann, H.: First Quantification of Imidazoles in
554 Ambient Aerosol Particles: Potential Photosensitizers, Brown Carbon Constituents, and Hazardous Components,
555 *Environ. Sci. Technol.*, 50, 1166-1173, <https://doi.org/10.1021/acs.est.5b05474>, 2016.

556 Teich, M., van Pinxteren, D., Wang, M., Kecorius, S., Wang, Z. B., Muller, T., Mocnik, G., and Herrmann, H.:
557 Contributions of nitrated aromatic compounds to the light absorption of water-soluble and particulate brown carbon in
558 different atmospheric environments in Germany and China, *Atmos. Chem. Phys.*, 17, 1653-1672,
559 <https://doi.org/10.5194/acp-17-1653-2017>, 2017.

560 Thieringer, J. R. D., Szabadi, J., Meyer, J., and Dittler, A.: Impact of Residential Real-World Wood Stove Operation
561 on Air Quality concerning PM_{2.5} Immission, Processes, 10, 545, <https://doi.org/10.3390/pr10030545>, 2022.

562 Wang, Q., Ye, J., Wang, Y., Zhang, T., Ran, W., Wu, Y., Tian, J., Li, L., Zhou, Y., Hang Ho, S. S., Dang, B., Zhang,
563 Q., Zhang, R., Chen, Y., Zhu, C., and Cao, J.: Wintertime Optical Properties of Primary and Secondary Brown Carbon
564 at a Regional Site in the North China Plain, *Environ. Sci. Technol.*, 53, 12389-12397,
565 <https://doi.org/10.1021/acs.est.9b03406>, 2019a.

566 Wang, Q. Y., Han, Y. M., Ye, J. H., Liu, S. X., Pongpiachan, S., Zhang, N. N., Han, Y. M., Tian, J., Wu, C., Long, X.,
567 Zhang, Q., Zhang, W. Y., Zhao, Z. Z., and Cao, J. J.: High Contribution of Secondary Brown Carbon to Aerosol Light
568 Absorption in the Southeastern Margin of Tibetan Plateau, *Geophys. Res. Lett.*, 46, 4962-4970,
569 <https://doi.org/10.1029/2019gl082731>, 2019b.

570 Wu, G., Wan, X., Gao, S., Fu, P., Yin, Y., Li, G., Zhang, G., Kang, S., Ram, K., and Cong, Z.: Humic-like substances
571 (HULIS) in aerosols of central Tibetan Plateau (Nam Co, 4730 m asl): Abundance, light absorption properties and
572 sources, *Environ. Sci. Technol.*, 52, 7203–7211, <https://doi.org/10.1021/acs.est.8b01251>, 2018.

573 Xie, M., Chen, X., Hays, M. D., Lewandowski, M., Offenberg, J., Kleindienst, T. E., and Holder, A. L.: Light
574 Absorption of Secondary Organic Aerosol: Composition and Contribution of Nitroaromatic Compounds, *Environ. Sci.*
575 *Technol.*, 51, 11607– 11616, <https://doi.org/10.1021/acs.est.7b03263>, 2017.

576 Xu, J. Z., Hettiyadura, A. P. S., Liu, Y. M., Zhang, X. H., Kang, S. C., and Laskin, A.: Regional Differences of
577 Chemical Composition and Optical Properties of Aerosols in the Tibetan Plateau, *J. Geophys. Res.-Atmos.*, 125,
578 e2019JD031226, <https://doi.org/10.1029/2019jd031226>, 2020.

579 Yang, Z., Tsona, N. T., George, C., and Du, L.: Nitrogen-Containing Compounds Enhance Light Absorption of
580 Aromatic-Derived Brown Carbon, *Environ. Sci. Technol.*, 56, 4005-4016, <https://doi.org/10.1021/acs.est.1c08794>,
581 2022.

582 Yus-Díez, J., Bernardoni, V., Mocnik, G., Alastuey, A., Ciniglia, D., Ivancic, M., Querol, X., Perez, N., Reche, C.,
583 Rigler, M., Vecchi, R., Valentini, S., & Pandolfi, M.: Determination of the multiple-scattering correction factor and its
584 cross-sensitivity to scattering and wavelength dependence for different AE33 Aethalometer filter tapes: a multi-
585 instrumental approach, *Atmos. Meas. Tech.*, 14: 6335-55, <https://doi.org/10.5194/amt-14-6335-2021>, 2021.

586 Zeng, L. H., Zhang, A. X., Wang, Y. H., Wagner, N. L., Katich, J. M., Schwarz, J. P., Schill, G. P., Brock, C., Froyd,
587 K. D., Murphy, D. M., Williamson, C. J., Kupc, A., Scheuer, E., Dibb, J., and Weber, R. J.: Global Measurements of
588 Brown Carbon and Estimated Direct Radiative Effects, *Geophys. Res. Lett.*, 47, <https://doi.org/10.1029/2020gl088747>,
589 2020.

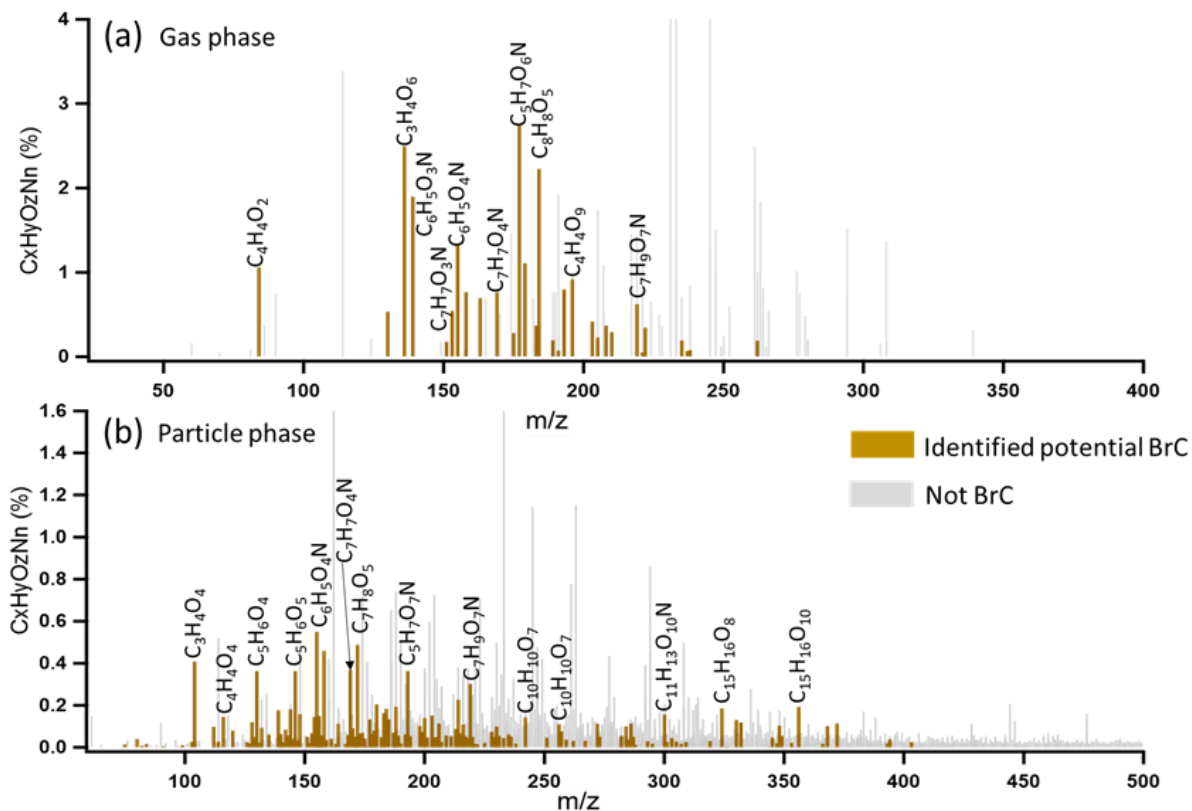
590 Zhang, Y., Albinet, A., Petit, J.-E., Jacob, V., Chevrier, F., Gille, G., Pontet, S., Chrétien, E., Dominik-Sègue, M.,
591 Levigoureux, G., Močnik, G., Gros, V., Jaffrezo, J.-L., and Favez, O.: Substantial brown carbon emissions from
592 wintertime residential wood burning over France, *Sci. Total Environ.*, 743, 140752,
593 <https://doi.org/10.1016/j.scitotenv.2020.140752>, 2020.

594 Zotter, P., H. Herich, M. Gysel, I. El-Haddad, Y. Zhang, G. Močnik, C. Hüglin, U. Baltensperger, S. Szidat, and A. S.
595 H. Prévôt. 2017.: Evaluation of the absorption Ångström exponents for traffic and wood burning in the Aethalometer-
596 based source apportionment using radiocarbon measurements of ambient aerosol, *Atmos. Chem. Phys.*, 17, 4229-49,
597 <https://doi.org/10.5194/acp-17-4229-2017>, 2017.

598

599

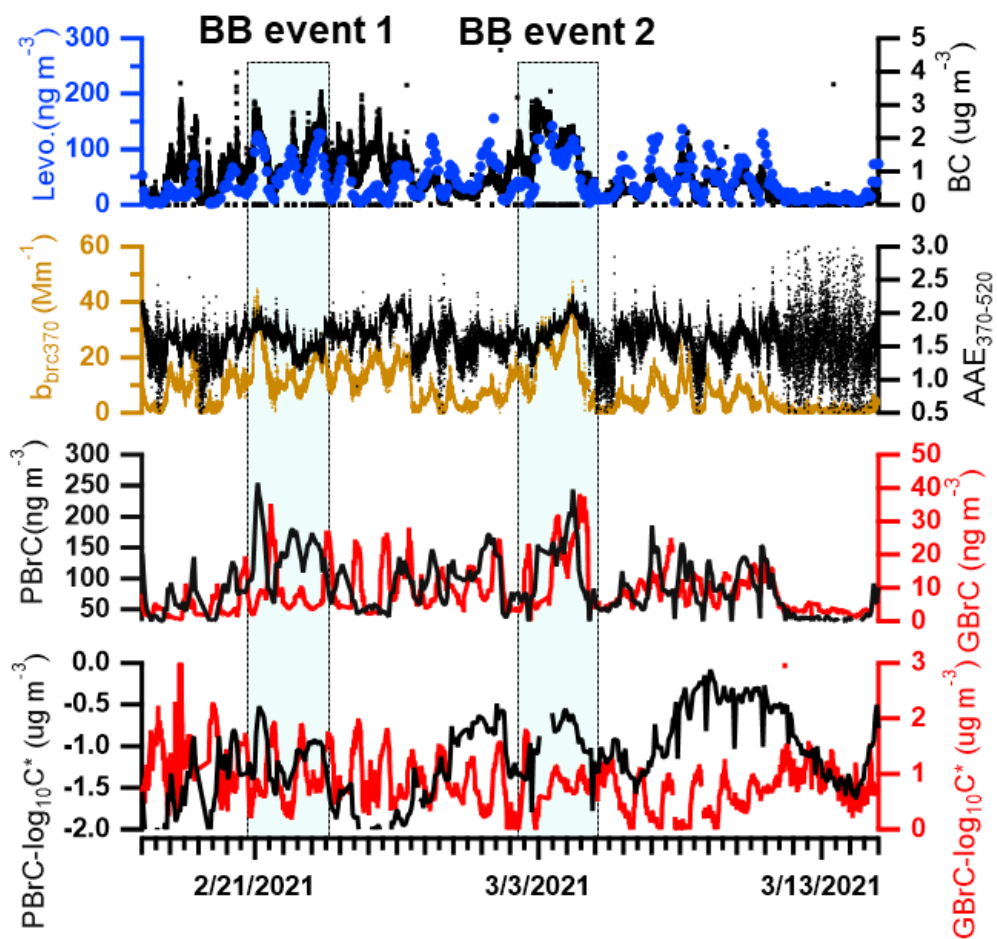
600



601

602 **Figure 1. CIMS mass spectra of organic aerosol measured by FIGAERO-CIMS for a biomass burning event on**
 603 **March 1st, 2021, a: gas phase, b: particle phase. The CI source employs reactions of I⁻ ions, which convert**
 604 **analyte molecules into [M+I]⁻ ions. Legends above MS features correspond to neutral molecules. The brown**
 605 **peaks in mass spectra were assigned as potential BrC molecules, while the gray peaks refer to the other organic**
 606 **molecules.**

607



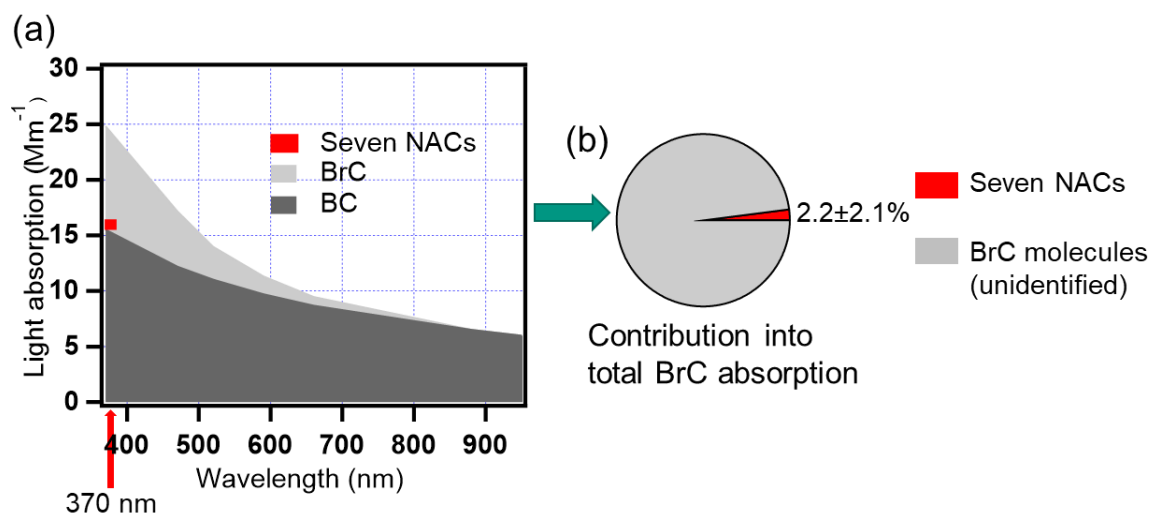
608

609 **Figure 2.** Time series of levoglucosan (Levo.) concentrations in particle phase from FIGAERO-CIMS, BC
 610 concentrations from aethalometer (AE33), absorption of brown carbon at 370 nm ($b_{\text{rc}370}$), absorption Ångström
 611 exponents between 370 nm and 520 nm ($\text{AAE}_{370-520}$), brown carbon concentrations in particle phase (PBrC) and
 612 gas phase (GBrC) and volatility ($\log_{10}C^*$) of brown carbon in particle phase (PBrC- $\log_{10}C^*$) and gas phase
 613 (GBrC- $\log_{10}C^*$) during the winter campaign.

614

615

616

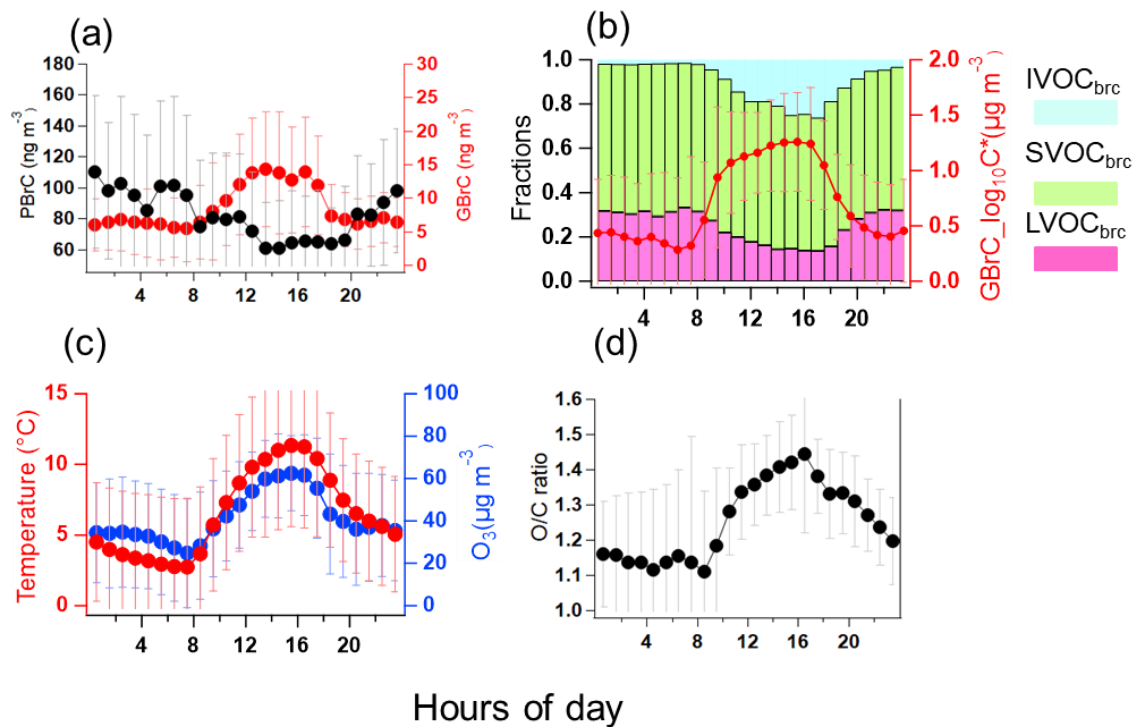


617

618 **Figure 3. (a) A stacked plot showing the main contributions to aerosol absorption from brown carbon and black**
619 **carbon based on the seven wavelengths measured by the aethalometer AE33. The contribution of seven NACs**
620 **to the total aerosol absorption is indicated in red at 370 nm. (b) Average absorption contribution of seven NACs**
621 **to total absorption by BrC. The red: seven NACs; the gray: unidentified-BrC molecules.**

622

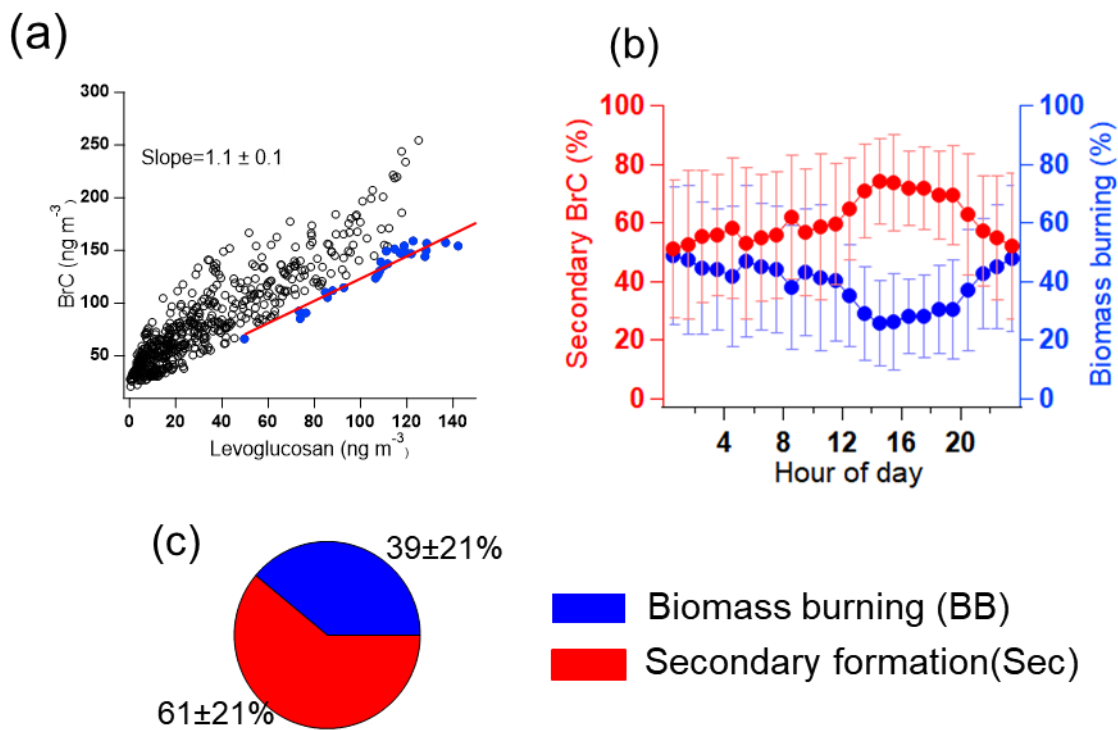
623



624
 625 **Figure 4. Diurnal profiles averaged over the whole winter campaign of (a) BrC in the particle (PBrC) and gas**
 626 **phase (GBrC), (b) BrC volatility fractions in LVOC_{brc}, SVOC_{brc}, IVOC_{brc}, and mean BrC volatility in the gas**
 627 **phase (red line), (c) temperature and ozone concentration. (d) O/C ratio of the oxidized organic components in**
 628 **the gas phase.**

629

630

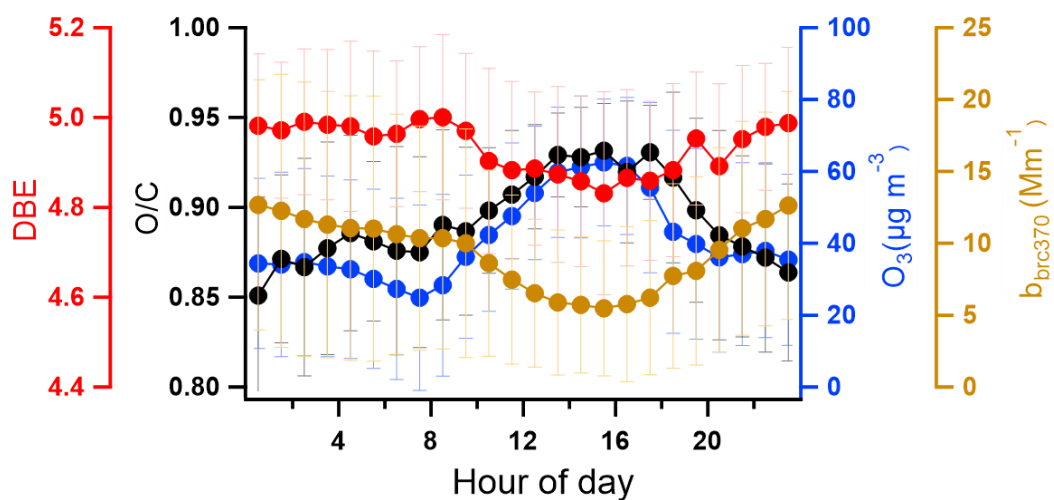


631
 632 **Figure 5. (a) Correlation analysis of BrC and levoglucosan in the particle phase for the analysis of the**
 633 **contribution of biomass burning using the edge method (Day et al., 2015). Blue points are the data used to**
 634 **determine [BrC/lev.]_{BB}. (b) diurnal profile of secondary-formation BrC and biomass-burning BrC for the whole**
 635 **measurement campaign. (c) Average mass fractions of secondary formed BrC and biomass-burning primary**
 636 **BrC for the whole campaign.**

637

638

639



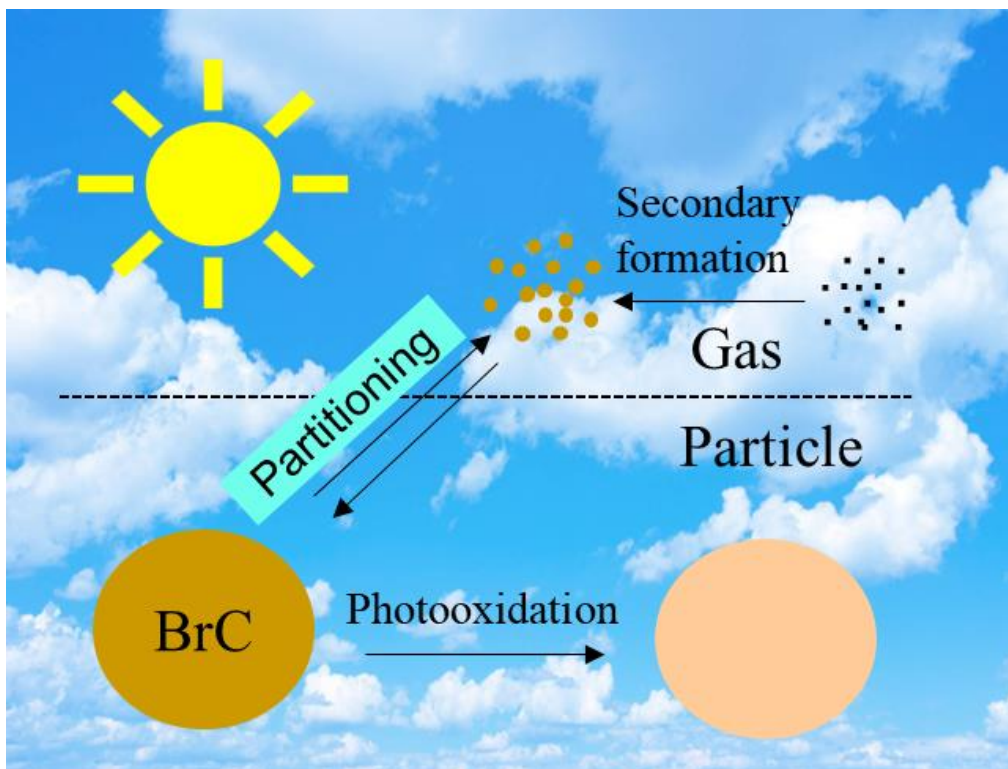
640

641 **Figure 6. The diurnal profile of DBE (double bond equivalent), O/C ratio of BrC, O₃, and b_{brc370} (absorption of**
642 **BrC at 370 nm) during the whole measured period.**

643

644

645



646

647 **Figure 7. A conceptual picture of the abstract**

648

649

650